BBAA VI International Colloquium on:
Bluff Bodies Aerodynamics & Applications
Milano, Italy, July, 20-24 2008

EXTENDED LATTICE BOLTZMANN EQUATION FOR SIMULATION OF FLOWS AROUND BLUFF BODIES IN HIGH REYNOLDS NUMBER

Tiancheng Liu*, Gao Liu*, Yaojun Ge†, Hongbo Wu*, Wenming Wu*

* China Highway Planning and Design Institute Consultants Co., Ltd., Beijing 100010, China
e-mail: liutcmail@126.com

† Tongji University, Shanghai 200092, China

Abstract: The Lattice Boltzmann method, a molecule kinetic-based approach, is presented to solve fluid dynamics. Based on the theory of turbulence and molecule kinetics, an extended Lattice Boltzmann equation is put forward to solve turbulent flow with high Reynolds number, in which sub-grid turbulence model is used to simulate vortex viscosity as well as turbulence relaxation time is introduced to modify the normal LBGK equation. The method to evaluate the turbulence relaxation time with particle distribution function is proposed combining with Smagorinsky turbulence model. Further more, the extended Lattice Boltzmann method is applied to simulate the flows around square cylinder in the range of Reynolds number from 10 to 100,000 and circular cylinder with Reynolds numbers from 10 to 140,000.

Keywords: Extended Lattice Boltzmann Equation, Turbulence Flow, High Reynolds number, Square cylinder, Circular cylinder

1 INTRODUCTION

Bluff body like square cylinder and circular cylinder have been widely used in practical engineering, such as bridge, high-rise building, water conservancy and so forth. Its prototype Reynolds number is often greater than 1×10^4 companying with turbulence flow and a wide range of technical aspects have been proposed ranging from experimental techniques over aerodynamics and structural dynamics to guidelines for the studies of square cylinder and circular cylinder [1-5]. Moreover, Numerical fluid dynamic (CFD) models and computer capacity have developed over the past two decades to a stage where assessment of the effect of practical cross-section shapes on structure response is possible [6]. In particular, numerical simulations appear well suited for design studies of the effect of cross-section shape on structure response to wind loading, thus presenting an efficient tool for weeding out inefficient cross-sections before embarking on confirmatory wind tunnel testing. Ref. [7-10] predicted successfully the flows around square cylinder and circular cylinder based on Navier-Stokes (NS) equations like Reynolds Averaged Navier-Stokes equation (RANS) and Large Eddy Simulation (LES). Walther, Larsen and Zhou applied the two-dimension discrete vortex method (DVM) to solve the aerodynamics of bluff body like bridge deck section [11-13]. LES technique recently has become a powerful tool for turbulent flow analysis in the field of computational wind engineering with the development of computer [6, 14-16]. LES is

much less sensitive to modeling errors since only the small sub-grid scales of motion are modeled. However, the computational cost of resolving turbulent boundary layers will constrain LES to moderate Reynolds number regimes for the foreseeable future [17]. However, the above mentioned methods are all on the basis of coarse grained model: Navier-Stokes equations, and the solution of these basic coarse-grained equations becomes mathematically difficult in the presence of turbulence, in which the simplified turbulence model used to modify the underlying coarse-grained equations still can not reliably reproduce many physical effects[17-18].

Here, we will analyze the molecule kinetic-based Lattice Boltzmann method (LBM), a new approach with different conception [19]. The Lattice Boltzmann method is an effective numerical scheme for solving complex fluid dynamics problems, which was firstly proposed by McNamara and Zanetti on the basis of Lattice Gas Automata (LGA) [20], and it has gained rapid progress in developing and employing in the last two decades [18, 21-25]. Unlike the conventional CFD methods, Lattice Boltzmann method is simpler to model complex physics first at the kinetic level, and then solve the appropriately modeled kinetic equations numerically. The macroscopic quantities including velocity and pressure are obtained by the moment integral of dynamical variables like distribution function [23]. It is assume that the details of the true collision operator that describes the interactions among eddies is immaterial. Lattice Boltzmann method is a time-dependent solver and provides an efficient scheme for the simulation of complex fluid dynamics.

There are several additional advantages using the Lattice Boltzmann method [26]. The Lattice Boltzmann method can avoid from nonlinear convection operator because of the simple advection combined with collision operator. The pressure can be easily obtained by an equation of state. The computations of the macroscopic quantities which relate the microscopic distribution function are extremely simple. The Lattice Boltzmann method is suitable for parallel computing due to the explicit and local algorithms which only depends on nearest neighbor information. Because of these attractive advantages, the Lattice Boltzmann method has been applied to simulate the multi-component flow, multiphase flow, suspension particle and others.

This paper, based on the theory of turbulence and molecule kinetics, an extended Lattice Boltzmann equation (ELBE) is developed combined with the turbulence model to simulate the flow around bluff bodies, and the Smagorinsky sub-grid model is employed to represent the contribution of small-scale flow. Further more, the extended Lattice Boltzmann method (ELBM) is applied to simulate the flows around the typical bluff bodies in various Reynolds number, saying square cylinder and circular cylinder. Finally, a summary of the computational results and discussion is concluded.

2 EXTENDED LATTICE BOLTZMANN EQUATION

2.1 Lattice Boltzmann Equation

It is thought that the flows are consisted of lots of particles in heat motion, and the behavior of many particle kinetic systems can be expressed as Boltzmann equation governing the single particle motions at molecular scales [21], namely,

$$\frac{\partial f}{\partial t} + \mathbf{v} \cdot \frac{\partial f}{\partial \mathbf{x}} = \Omega(f) \tag{1}$$

where $f = f(\mathbf{x},\mathbf{v},t)$ is the particle distribution function; $\mathbf{v}$ is the particle velocity vector; $\mathbf{x}$ is the spatial position; t is the time variable. The left-hand side of Eq. (1) represents the free streaming of molecules in space while the right-hand side expresses intermolecular

interactions or collisions. On the assumption that the details of the collision operator are immaterial, an effective collision operator represented by BGK (Bhatnagar-Gross-Krook [27]) expression is introduced as follows,

$$\frac{\partial f}{\partial t} + \mathbf{v} \cdot \nabla f = -\frac{1}{\lambda}(f - f^{(eq)}) \tag{2}$$

where λ is the relaxation time; $f^{(eq)}$ is the equilibrium distribution function. In Eq. (2), described essential physics of molecular interactions, the collision operator involves a simple relaxation to a local equilibrium distribution $f^{(eq)}$ with a characteristic time scale λ.

To solve f numerically, Eq. (2) should be discretized in the velocity space with a finite set of velocity vectors $\{e_\alpha\}$ in the content of conservation laws, and then a completely discretized equation is derived with the time step Δt and space step $\Delta \mathbf{x}$, called as LBGK equation [21,23],

$$f_\alpha(\mathbf{x}_i + \mathbf{e}_\alpha \Delta t, t + \Delta t) - f_\alpha(\mathbf{x}_i, t) = -\frac{1}{\tau}\left[f_\alpha(\mathbf{x}_i, t) - f_\alpha^{(eq)}(\mathbf{x}_i, t)\right] \tag{3}$$

where f_α is the particle distribution function associated with the αth discrete velocity $\mathbf{e}_\alpha$; $\mathbf{x}_i$ is the location of spatial points; and $\tau = \lambda / \Delta t$ is the dimensionless relaxation time.

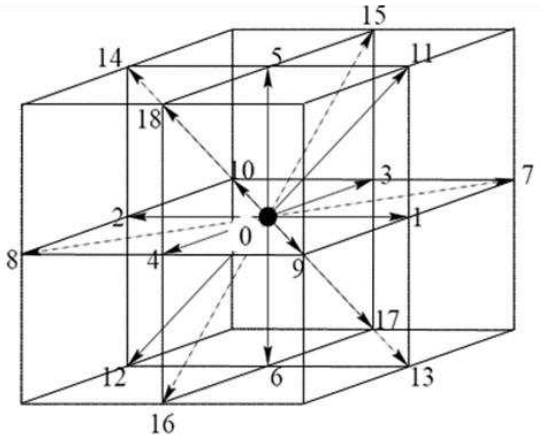

Figure 1: Topological structure of D3Q19 lattice model

Here, Eq. (2) is discretized with nineteen-velocity vectors and cube grid structure shown as figure 1, which is referred to as the D3Q19 model [23]. The equilibrium distribution function is of the form:

$$f_\alpha^{(eq)} = w_\alpha \rho \left[1 + \frac{3}{c^2}\mathbf{e}_\alpha \cdot \mathbf{u} + \frac{9}{2c^4}(\mathbf{e}_\alpha \cdot \mathbf{u})^2 - \frac{3}{2c^2}\mathbf{u} \cdot \mathbf{u}\right] \tag{4}$$

where w_α is the weighting factors given by $w_0 = 1/3$, $w_{1\sim6} = 1/18$, and $w_{7\sim18} = 1/36$; $c = \Delta x / \Delta t$ is the speed of particle; and the fluid density ρ and velocity $\mathbf{u}$ are evaluated by $\rho = \sum f_\alpha$ and $\rho \mathbf{u} = \sum \mathbf{e}_\alpha f_\alpha$, respectively. The pressure should be calculated by the state formula $p = c_s^2 \rho$, in which $c_s = c/\sqrt{3}$ is the speed of sound for this model. The viscosity of flow depends on the speed of sound and relaxation time, i.e. $\nu = c_s^2(\tau - 1/2)\Delta t$. When the Knudsen number Kn<<1, NS equations could been derived from Lattice Boltzmann equation by using multi-scale Chapman-Enskog expression [28] in the content of the conservation principles of mass.

2.2 Incorporating turbulence model into LB equation

In general, turbulence is composed of large-scale flow and small-scale fluctuation, and the energy cascades from large-scale flow down to small-scale fluctuation [17, 18]. Here turbulence theory is being applied to account for the eddy viscosity of all scales of turbulent motion even the anisotropic scales, and the eddy viscous turbulence model is introduced to the normal LBE. The large-scale flow is solved exactly by the particle distribution function f and the equilibrium distribution function $f^{(eq)}$. This solved-scale flow determines the local effective relaxation time to account for the unresolved-scale turbulent motion in the Boltzmann collision. Then, the total relaxation time τ_{total} is locally determined for each cell in the simulation domain for each time–step via the supplementary sub-grid turbulence model. Indeed, the total relaxation time τ_{total} depends on the variety of different turbulent physics, including the molecule viscosity υ_0 and eddy viscosity υ_t. Thus, the total relaxation time τ_{total} is composed of two parts, the molecule relaxation τ_0 depending on υ_0 and the turbulence relaxation time τ_t due to υ_t. Consequently, the relaxation time τ in Eq. (3) can be replaced by the total relaxation time τ_{total}, and the Eq. (3) can be modified as follows,

$$f_\alpha(\mathbf{x}+\mathbf{e}_\alpha\Delta t, t+\Delta t) = f_\alpha(\mathbf{x},t) - \frac{1}{\tau_{total}}(f_\alpha - f_\alpha^{(eq)}) \tag{5}$$

where $\tau_{total}=\tau_0+\tau_t$ depends on the space and time.

The remaining problem is to determine the effective total relaxation time τ_{total} describing the dynamics of turbulent fluctuations. Due to the relationship of relaxation time and viscosity of flow, the total relaxation time can be expressed as this formula, i.e.

$$\tau_{total} = 3\frac{\Delta t}{\Delta x^2}(\upsilon_0 + \upsilon_t) + \frac{1}{2} \tag{6}$$

The eddy viscosity υ_t is governed by the Smagorinsky model [6],

$$\upsilon_t = (C_s\Delta)^2\left|\bar{S}\right| \tag{7}$$

where C_s is a Smagorinsky constant; □ is the filter size; and $|\bar{S}| = \sqrt{2\bar{S}_{ij}\bar{S}_{ij}}$ is the magnitude of the strain-rate tensor $\bar{S}_{ij}$. The $\bar{S}_{ij}$ can be evaluated with resolved-scale non-equilibrium momentum tensor,

$$\bar{S}_{ij} = -\frac{3}{2\rho\tau_{total}\Delta t}\prod_{ij}^{(1)} \tag{8}$$

where $\prod_{ij} = \sum_\alpha e_{\alpha i}e_{\alpha j}(f_\alpha - f_\alpha^{eq})$. Then, the eddy viscosity is expressed as

$$\upsilon_t = \frac{3}{\sqrt{2}\bar{\rho}\tau_{total}\Delta t}(C_s\Delta)^2\sqrt{\bar{Q}} \tag{9}$$

where $\bar{Q} = \bar{\prod}_{ij}\bar{\prod}_{ij}$. Consequently, the total relaxation time τ_{total} can be solved by

$$\tau_{total} = \frac{1}{2}\left(\sqrt{\tau_0^{\,2} + \frac{18}{\Delta x^2\bar{\rho}}(C_s\Delta)^2\sqrt{2\bar{Q}}} + \tau_0\right) \tag{10}$$

There exists great difference between the behaviors of turbulence model in present ELBM and NS models e.g. RANS and LES. In NS solvers, the turbulence model is used as the complement to averaged NS equations; the effect of the eddy viscosity is instantaneous; and the non-hydrodynamic variables are completely neglected. Whereas the LBE can be solved exactly without turbulence model, the sub-grid stress is not instantly in equilibrium which can lead to more spatial-temporal memory effects. Even without changing the turbulence model for fluctuating eddies, the LBM has already extended the physical range of application for

realistic modeling of large-scale flows due to the fact that large and small (sub-grid) scales are not separated.

2.3 Parallel simulation process

A parallel Lattice Boltzmann algorithm that is suitable for muster-computers is developed, and the parallel computation code is compiled using C++ computer language.

During the solution of Eq. (5), it can be separated into two steps according to the movement process of particle, collision and transfer showing as follows.

$$\text{Collision step:}\quad \tilde{f}_\alpha(\mathbf{x}_i,t+\Delta t)=f_\alpha(\mathbf{x}_i,t)-\frac{1}{\tau_{total}}\left[f_\alpha(\mathbf{x}_i,t)-f_\alpha^{(eq)}(\mathbf{x}_i,t)\right] \qquad (11a)$$

$$\text{Transfer step:}\quad f_\alpha(\mathbf{x}_i+\mathbf{e}_\alpha\Delta t,t+\Delta t)=\tilde{f}_\alpha(\mathbf{x}_i,t+\Delta t) \qquad (11b)$$

where $\tilde{f}_\alpha$ denotes the particle state after collision operation.

In this way, the numerical computation process can be illustrated as figure 2.

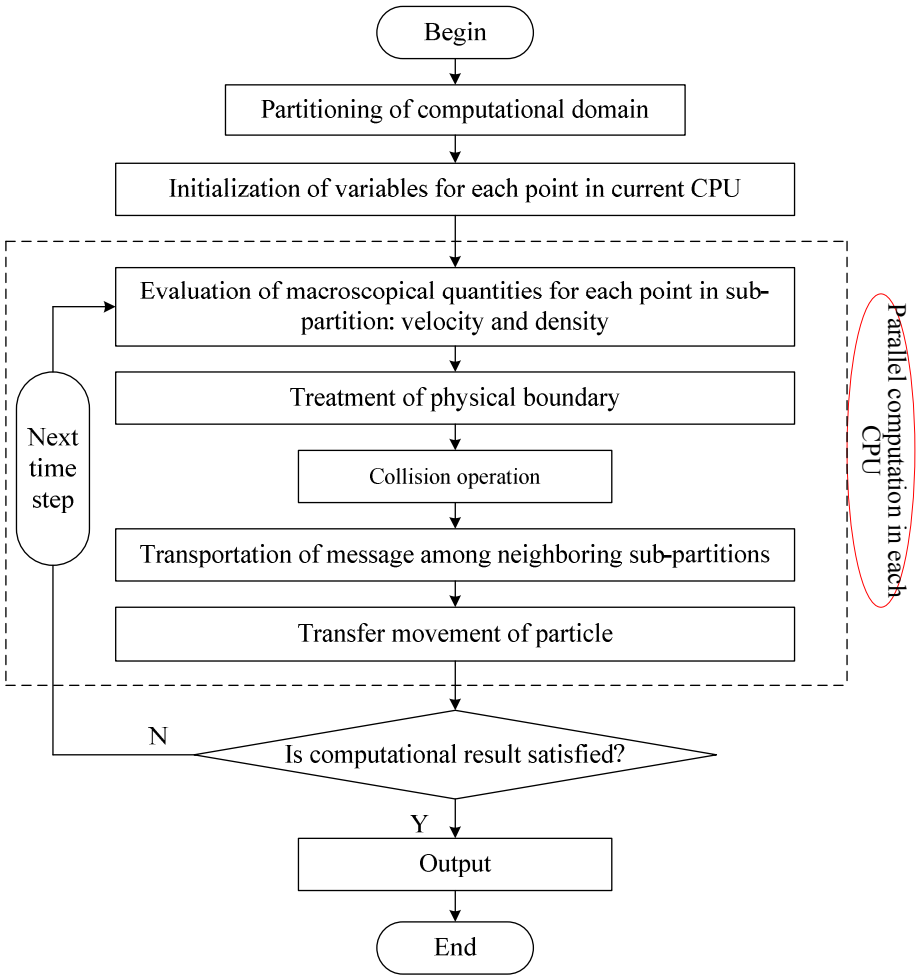

Figure 2: Parallel computation process

(a) the computational domain is divided into several sub-partition which is computed by corresponding CPU; (b) Initialization of variables for each point; (c) evaluation of macroscopical quantities for each point: velocity and density; (d) treatment of physical boundary; (e) collision operation; (f) transportation of message among neighboring sub-partition; (g) transfer movement of particle; (h) iteration from (c) to (g) until the flow field is

meeting. During above computational procedure, the items (c), (d) and (e) are independent from other points while the item of (g) needs neighboring points. These characteristics give Lattice Boltzmann method the natural advantage of parallel computation with muster CPU.

3 SIMULATION OF FLOW AROUND SQUARE CYLINDER

3.1 Computational condition of square cylinder

The simulations of flows around square cylinder are performed in the range of Reynolds number from 10 to 10^5 based on the above mentioned ELBM.

The square cylinder is placed in a channel with uniform inflow shown as figure 3 and figure 4. The coordinate system is set as: the *x*, *y* and *z* axes are the stream-wise, lateral and span-wise directions, respectively. The computational domain covers 30D in stream-wise direction (-10<*x*/*D*<20), 20D in normal direction (-10<*y*/*D*<10) and 0.1D in span-wise direction. The velocity boundary condition is applied for inlet; the pressure boundary condition for outlet; the non-slip wall boundary conditions for the outer-wall of flow field; and periodic boundary conditions for z direction.

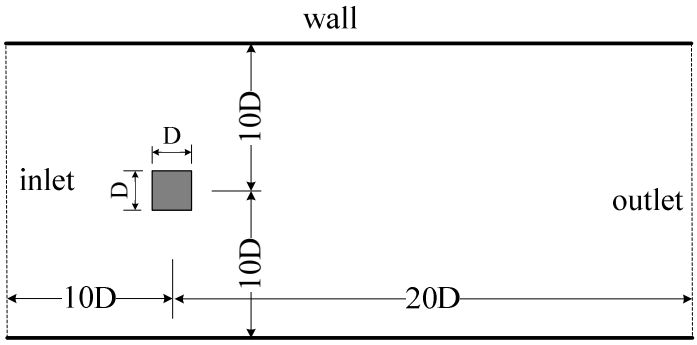

Figure 3: Computational domain of flow around square cylinder

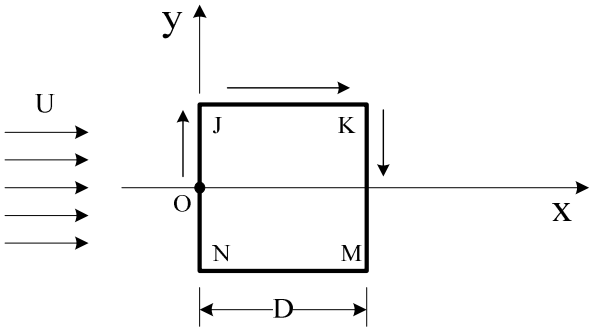

Figure 4: Coordinate for square cylinder

In these cases, the Reynolds number is defined as follows:

$$Re=Du/v \tag{12}$$

where u is the uniform inlet velocity and D is the width of square cylinder.

The computational results reported like wind loads and Strouhal number are made of dimensionless:

$$C_D = \frac{Fx}{\frac{1}{2}\rho u^2 DL} \tag{13}$$

$$St = \frac{fD}{u} \tag{14}$$

where C_D and St are the drag coefficient and Strouhal number, respectively; ρ is the density of flow; Fx is the aerodynamic forces on bluff body model in direction x; L is the length in span-wise directions; f is the frequency evaluated by the Fourier transform of lift time history; u is the inlet flow speed; D is the character length of obstacle.

3.2 Computational case of square cylinder at Re=22000

In the cases of flows around square cylinder, the computation at Re=22000 is performed to verify the validity of ELBM at first.

Table 1 lists the drag coefficient C_D and Strouhal number St. It shows that the present results agree well with that of experiments and LES method after detail comparison.

Method/source of result	C_D	St
Present results	2.084	0.140
Experiment (D.A. Lyn et al., 1995)	2.100	0.132
Experiment (D. Durão et al., 1988)	2.050□2.230	0.139
LES (S. Vengadesan, et al., 2005)	2.240	0.136

Table 1: Comparison of the drag coefficient and Strouhal number for square cylinder at Re=22000

Figure 5 (a) and (b) illustrate the distribution of the time-averaged stream-wise velocity component along the wake centerline and along axis y with x/D=0.5, respectively. These quantities are compared with that of Lyn's experiment, Durao's experiment and traditional CFD methods including LES and RANS. From which, we can find that the present results have good agreement with Lyn's and Durão's experimental results though it is litter high in the case of x/D>3; the mean stream-wise velocity along y direction at x/D=0.5 are in close proximity to that of experiment and LES.

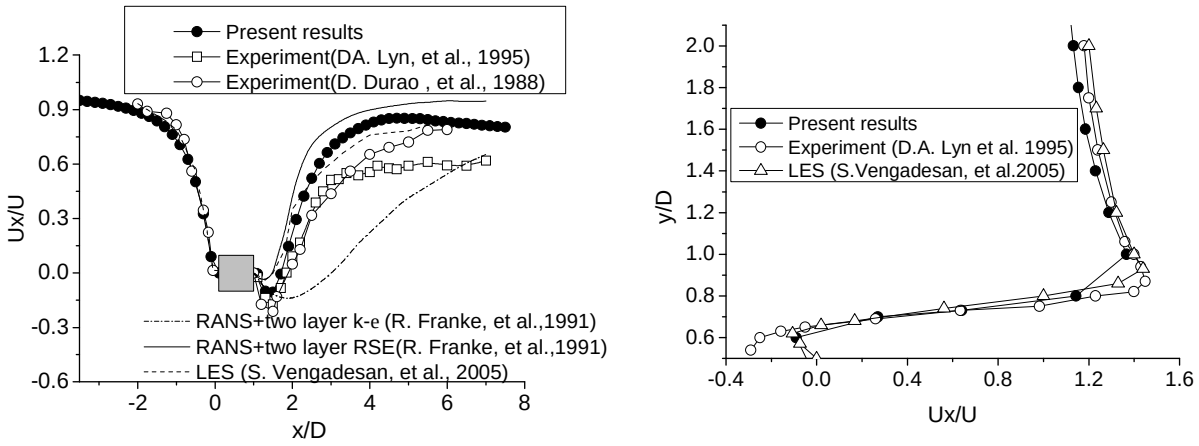

(a) Along the wake centerline

(b) On the square cylinder side, x/D=0.5

Figure 5: Comparison of the stream-wise component of mean velocity

The surface pressure coefficients around the body are shown as figure 6 compared with experimental data [1, 29] and discrete vortex method results [30], in which "s" is the length from the center of windward face and moving clockwise around the body referred to figure 4. It can be found that the present results are close to the experimental data. The present results appear more favorable compared with those derived from DVM calculations.

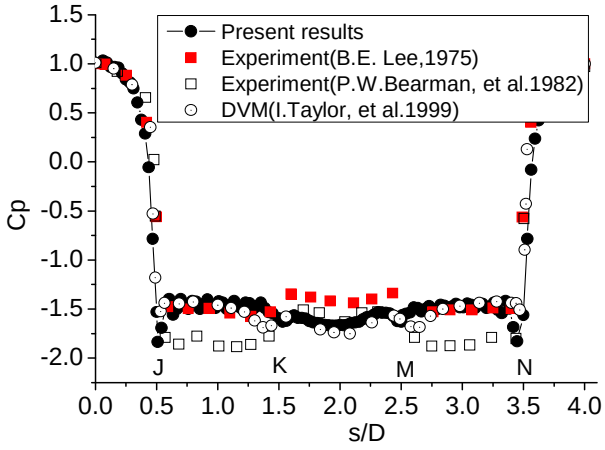

Figure 6: Comparison of surface pressure distribution

3.3 Reynolds number effects on square cylinder

The simulations are performed to study the Reynolds number effects on flows around square cylinder with range of Reynolds numbers from 10 to 1.0×10^5.

Figure 7 depicts the streamlines of the flow around square cylinder at various Reynolds numbers. It is visible that the flows are changing from laminar flows to turbulence flows with the increase of Reynolds numbers. The flow is steady when Reynolds number is less than about 65, and becomes periodic vortex shedding as the Reynolds number is greater than 65; when the Reynolds number is greater than 200, small-scale vortices occur on the side face as well as the separation points move to windward corners; the flow becomes instable at Re=500 approximately; with the increase of Reynolds number, the leeward main vortex becomes smaller while the flow becomes more and more complex with multi-level vortices.

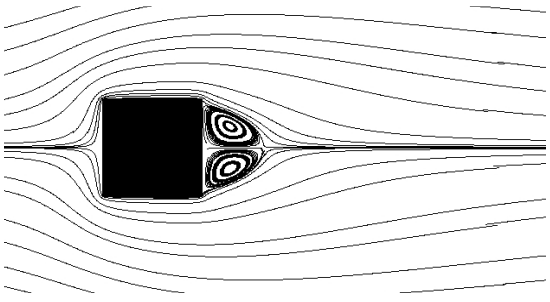

(a) Re=10

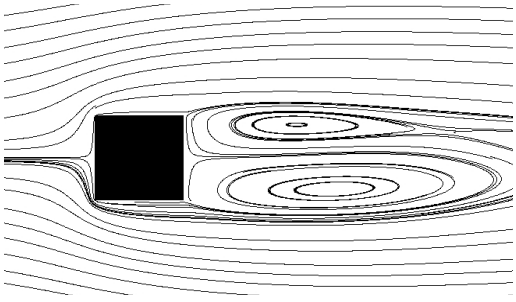

(b) Re=65

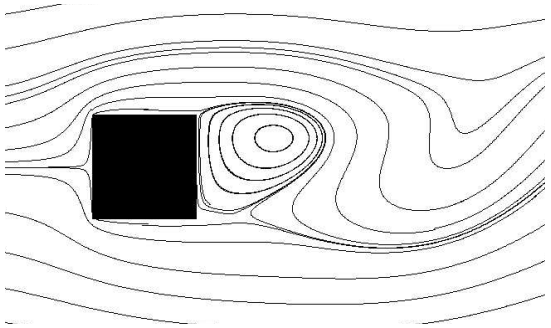

(c) Re=100

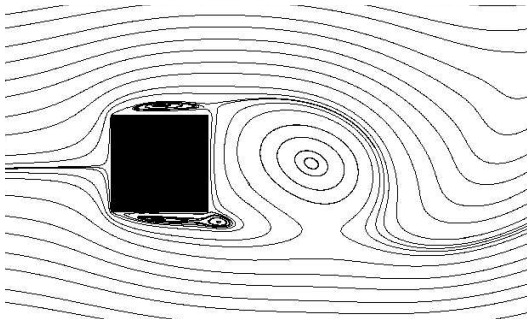

(d) Re=200

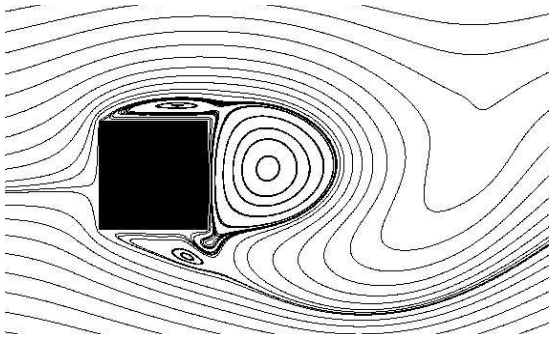

(e) Re=500

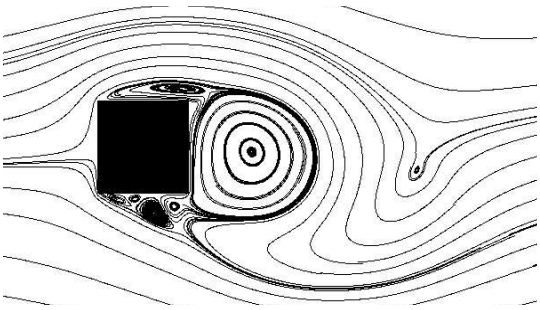

(f) Re=1000

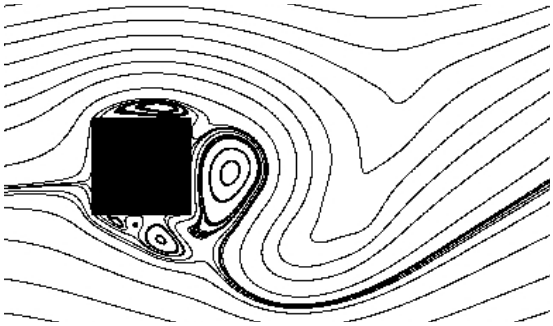

(g) Re=2.2×10^4

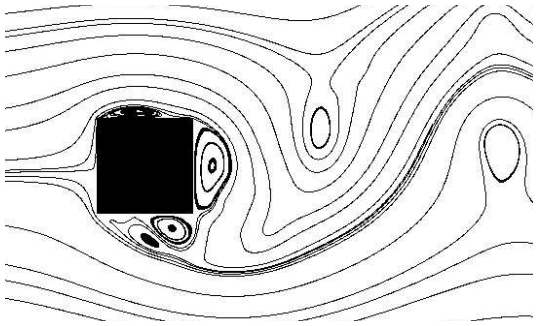

(h) Re=1.0×10^5

Figure 7: Comparison of surface pressure distribution

The drag coefficients C_D and Strouhal numbers for square cylinder are dependent on the Reynolds number as well, as shown in figure 8 and figure 9, respectively. The present results have good agreements with experimental results [7, 8] and other numerical results [5, 6, and 9]. The drag coefficients have sharp change while Re<5000 and tend to be 2.10 while Re>5000. The Strouhal numbers have also sharp variety in the range of Re<5000, and are closed to be 0.132 in the case of Re>5000.

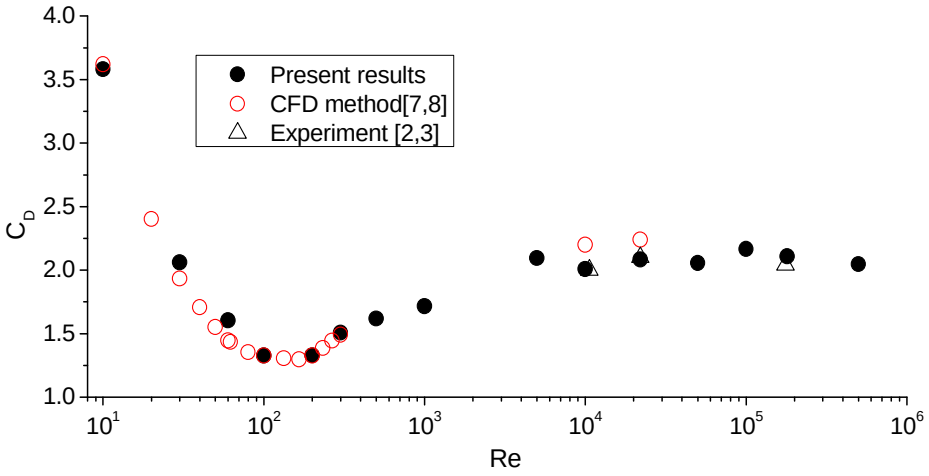

Figure 8: Drag coefficients depending on Reynolds number

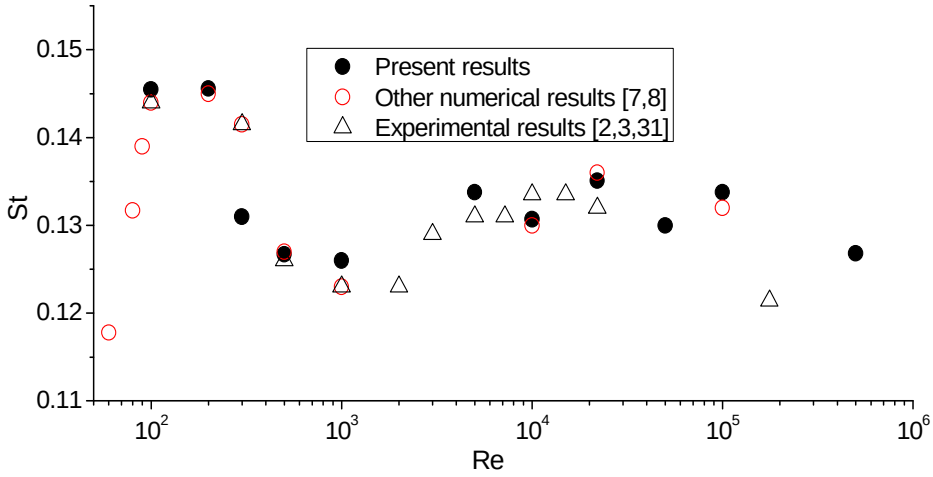

Figure 9: Strouhal number depending on Reynolds number

4 SIMULATION OF FLOW AROUND CIRCULAR CYLINDER

Circular cylinder is also a typical bluff body which is often used to verify numerical model. The simulations of flows around circular cylinder are performed in the range of Reynolds number from 10 to 1.4×10^5.

4.1 Computational condition of circular cylinder

The circular cylinder is set into a channel with uniform inflow speed u in the stream direction *x*. As shown in figure 10, the computation domain considered here is $-10D\leq x\leq 20D$, $-10D\leq y\leq 10D$ and $-0.5D\leq z\leq 0.5D$, where *D* is the diameter of circular cylinder. Velocity boundary condition is applied for inlet; the pressure boundary condition for outlet; non-slip wall boundary conditions for the exterior wall of flow field and surface of obstacle; periodic boundary conditions for z direction. The results about circular cylinder are reported in the same form as square cylinder defined as Eq. (13) and (14).

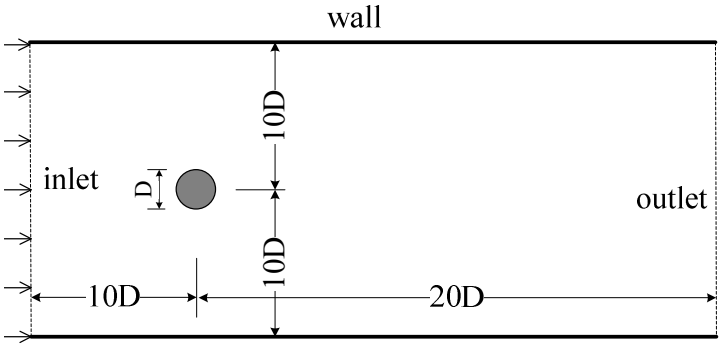

Figure 10: Computational domain of flow around square cylinder

4.2 Computational results of flows around circular cylinder

Table 2 lists the drag coefficient C_D and Strouhal number *St* comparing with that of experimental and traditional CFD methods like DVM, NS-LES and RANS. From which we can find the ELBM's results have good agreement with the referenced results while Reynolds numbers are equal to 200, 3900 and 1.4×10^5, respectively.

Re	method	C_D	*St*
200	Present results	1.34	0.198
	DVM (J.H. Walther, A. Larsen, 1997)	1.32	0.194
	FEM (F.C. Cao, 1999)	1.39	0.189
	Experiment (F.C. Cao, 1999)	1.300	0.190
3900	Present results	1.186	0.215
	Experiment (L.Ong, et al. 1996)	0.99±0.05	0.215±0.005
	LES (Kravchenko, et al. 2000)	1.000	0.203
	RANS + standard Algebraic Stress Models(SASM) (H. Lübcke, et al., 2001)	0.890	0.200
	RANS + Explicit Algebraic Stress Models(EASM) (H. Lübcke, et al., 2001)	0.980	0.203
1.4×10^5	Present results	1.259	0.209
	Experiment (B. Cantwell, et al. 1983)	1.237	0.200
	LES (M. Breuer, 1999)	1.239	0.204
	RANS+ Explicit Algebraic Stress Models(EASM) (H. Lübcke, et al., 2001)	1.160	0.220

Table 2: Drag coefficients and Strouhal number of circular cylinder depending on Re

In order to study the Reynolds number effects on flow around circular cylinder, a number of cases have been done in the range of Reynolds number from 10 to 10^5. Figure 11 shows the pressure isoline and streamlines which describe the details of flows around circular cylinder possessed of different Reynolds number. From which, it is visible that the flows are changing from laminar flow to turbulence with the increase of Reynolds number. In the case of Re=10, the flow is steady with light separation; when the Reynolds number equals to 40, there exists visible separation on the leeward face with steady symmetric vortices; the phenomenon of vortex shedding occurs at Re=100, which is often called as Karman vortex; with the increase of Reynolds number, there are more and more small-scale vortices appearing on the leeward face, and the flow becomes into turbulence.

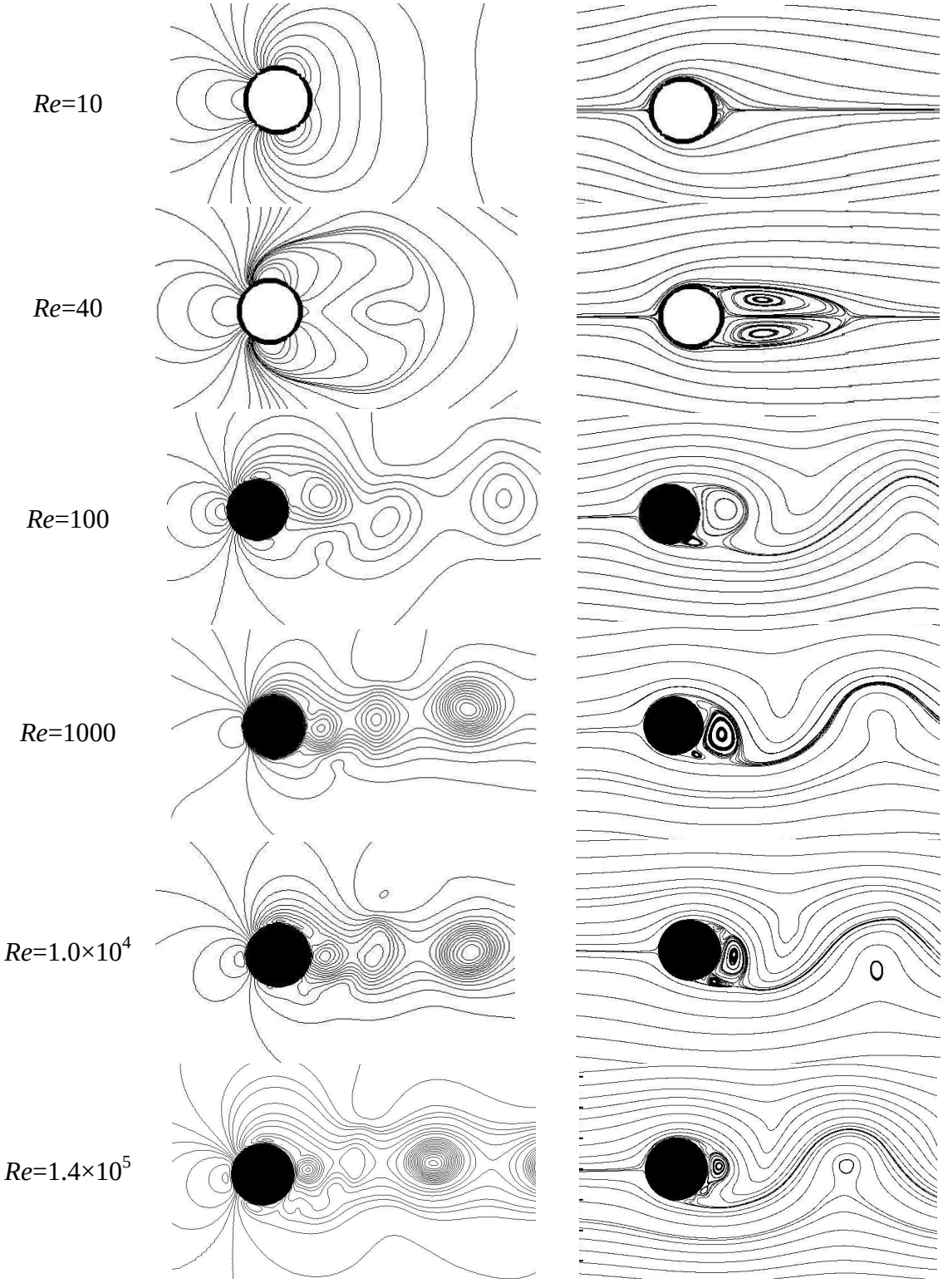

(a) Pressure field (b) streamline

Figure 11: Flow states of circular cylinder depending on Reynolds numbers

From figure 11, we can find the flows around circular cylinder vary periodically with the characteristic of symmetric vortex shedding when the Reynolds number belongs to the subcritical range, which is as same as reference [35]. This phenomenon can be visualized by

figure 12 showing the instantaneous streamline, pressure isoline and turbulence viscosity isoline of flow around circular cylinder with Re=3900.

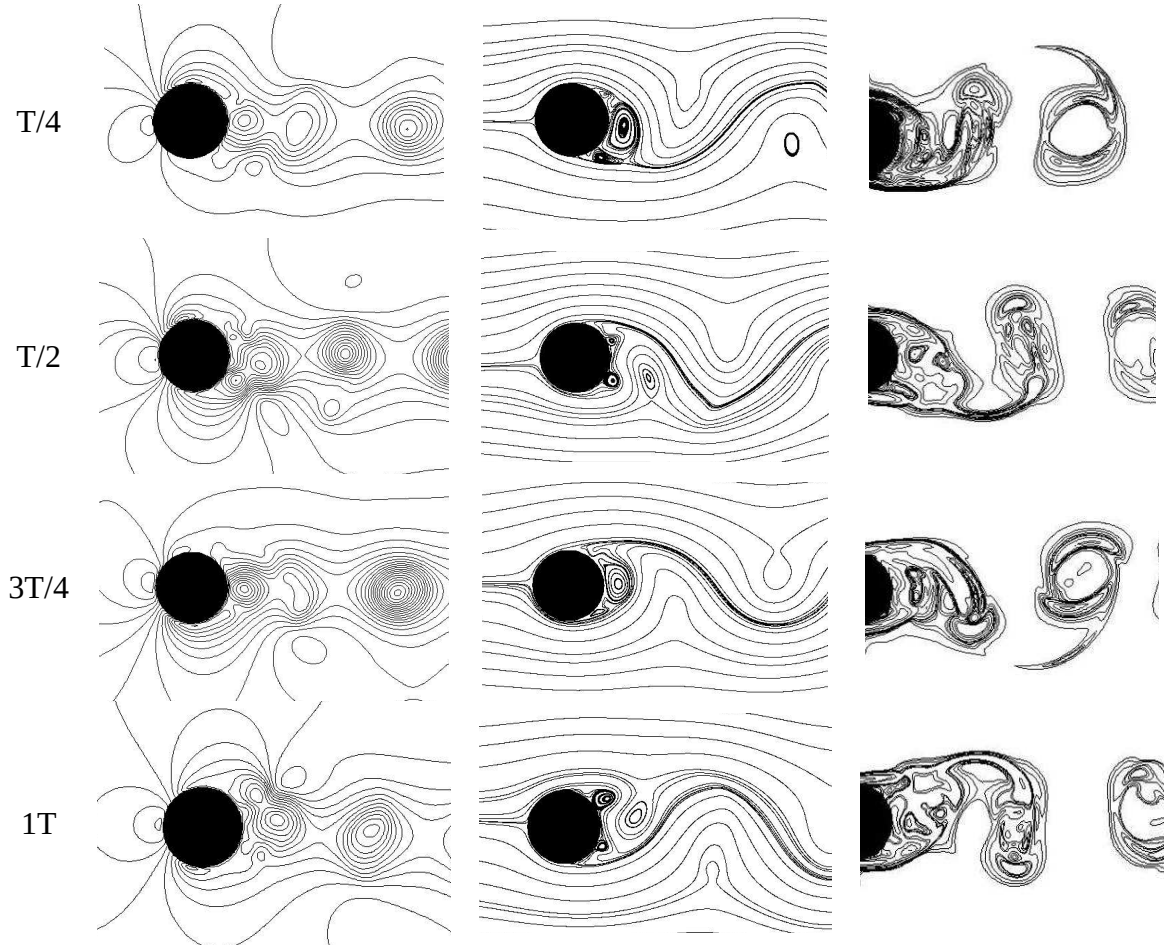

(a) Pressure isoline (b) Streamline (c) Turbulence viscosity

Figure 12: Periodic variety of flow around circular cylinder with Re=3900

The behavior of flow around circular cylinder mentioned above is described by drag coefficients C_D and Strouhal numbers as well, shown as figure 13 and figure 14, respectively. The drag coefficients is 1.95 for Re=10 and decreases immediately to 1.22 for Re=1000. However, the Strouhal number has inverse trend which increases from 0.17 at Re=100 to 0.21 at Re=1000. With the increase of Reynolds number, the drag coefficient tends to be 1.0~1.2 while the Strouhal number tends to be 0.20~0.22. Comparing with experimental results and other numerical results in the Ref. [33], it can be concluded that the present results agree well with benchmark.

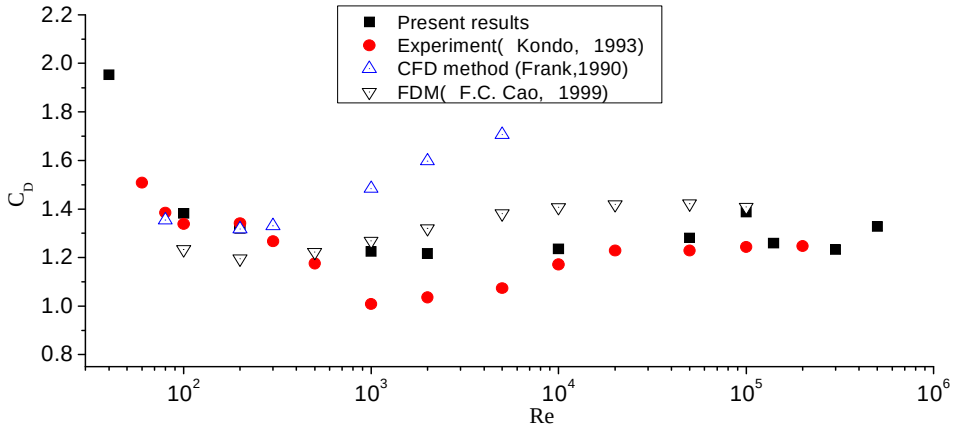

Figure 13: Drag coefficients of circular cylinder depending on Reynolds number

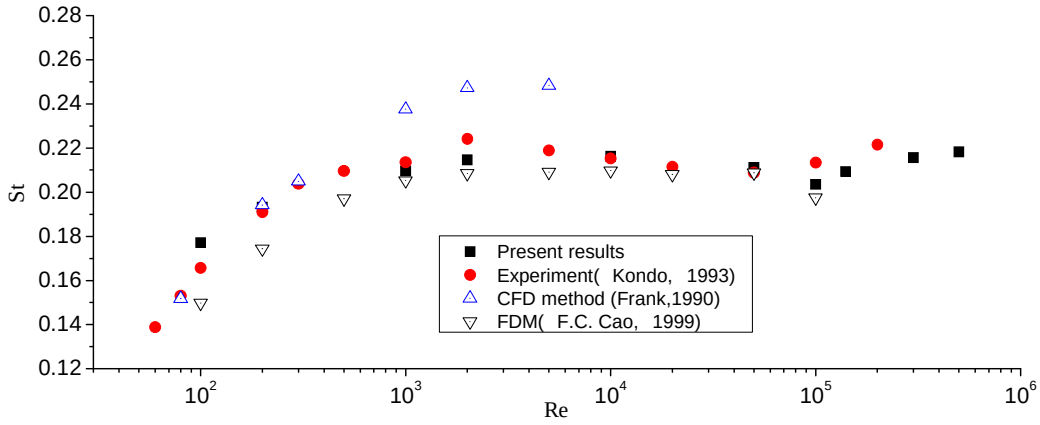

Figure 14: Strouhal number of circular cylinder depending on Reynolds number

5 CONCLUDING REMARKS

- The extended lattice Boltzmann equation is derived based on molecule kinetic theory and turbulence theory, which is verified by the simulation of flow around square cylinder at various Reynolds numbers.
- The extended Lattice Boltzmann equation is suitable not only for steady flow at low Reynolds number but also for unsteady flow at high Reynolds number.
- The flows around square cylinder and circular cylinder can be predicted correctively by present extended Lattice Boltzmann equation.
- In the cases of square cylinder and circular cylinder, the details of flow field depend on the Reynolds numbers as well as the drag and the vortexes shedding frequency.
- It is very important and significant for LB method as a green CFD approach to be applied to practical engineering.

ACKNOWLEDGEMENTS

The authors are grateful to the financial support by the National High-Tech Research and Development Plan of China (No. 2007AA11Z101) and the Western Region Science & Technology Development Projects, Ministry of Communication, China (No.2006318 49426, 2005318 00019).

REFERENCES

[1] B.E. Lee. The effect of turbulence on the surface pressure field of a square prism. *J. Fluid Mech*. 69, 1975, 263-282.

[2] D. Durão, M. Heitor, J. Pereira. Measurements of turbulent and periodic flows around a square cross-section cylinder. *J. Exp. Fluid*., **6**, 298–304, 1988.

[3] D.A. Lyn, S. Einva, W. Rodi, et al. A Laser-Doppler Velocimetry Study of Ensemble Averaged Characteristics of the Turbulent Near Wake of a Square Cylinder. *J. Fluid Mech.*, **304**, 285–319, 1995.

[4] L. Ong, J. Wallace. The velocity field of the turbulent very near wake of a circular cylinder, *Exp. Fluids* 20, 441, 1996.

[5] B. Cantwell, D. Coles. An experimental study of entrainment and transport in the turbulent wake of a circular cylinder. *J. Fluid Mech.*, 136, 321, 1983.

[6] T. Tamura. Towards practical use of LES in wind engineering. *CWE2006*, Yokohama, 1-8, 2006.

[7] R. Franke, W. Rodi. Calculation of vortex shedding past a square cylinder with various turbulence models. *Proceeding*: 8th Symp. Turbulent Shear Flows, Tech. Univ. Munich, Springer Berlin, 189-204, 1991.

[8] S. Vengadesan, A. Nakayama. Evaluation of LES models for flow over bluff body from engineering application perspective. Sadhana vol. 30, Part 1, India, 11-20, 2005.

[9] H. Lübcke, S. Schmidt, T. Rung, F. Thiele. Comparison of LES and RANS in bluff-body flows. *J. Wind. Eng. Ind. Aero*. , 89, 1471-1485, 2001.

[10] A.G. Kravchenko, P. Moin. Numerical studies of flow over a circular cylinder at Re=3900. *Phys. Fluid*., 12, 403-412, 2000.

[11] J.H. Walther. Discrete vortex method for two-dimensional flow past bodies of arbitrary shape undergoing prescribed rotary and translational motion. Ph.D. thesis, Department of fluid mechanics, Technical University of Denmark, AFM, 1994.

[12] A. Larsen and J.H. Walther. Aeroelastic analysis of bridge girder section based on discrete vortex simulations, *J. Wind. Eng. Ind. Aero*. , 67/68, 253-265, 1997.

[13] Z. Zhou, A. Chen, H. Xiang. On the mechanism of torsional flutter instability for 1st Tacoma Narrow Bridge by discrete vortex method, *CWE2006*, Yokohama, 505-508, 2006.

[14] A. Nakayama and H. Noda. LES simulation of flow around a bluff body fitted with a splitter plate. *J. Wind. Eng. Ind. Aero*. , 85, 85-96, 2000.

[15] D. Yu, A. Kareem. Parametric study of flow around rectangular prisms using LES. *J. Wind. Eng. Ind. Aero*. , 77/78, 653-662, 1998.

[16] Y. Ono, T. Tamura. Large eddy simulation using a curvilinear coordinate system for the flow around a square cylinder. *Wind and Structure*, 15(2), 369-378, 2002.

[17] P.R. Spalart. Strategies for turbulence modeling and simulations. *Int. J. Heat Fluid Flow*, **21**, 252–263, 2000.

[18] H.D. Chen, K. Satheesh, O. Steven, et al. Extended Boltzmann Kinetic Equation for Turbulent Flows. *SCIENCE*, **301**, 633–636, 2003.

[19] G.R. McNamara, G. Zanetti. Use of the Boltzmann Equation to Simulate Lattice Automata. *J. Phys. Rev. Let.*, **61**, 2332–2335, 1988.

[20] U. Frish, B. Hassalacher, Y. Pomeau. Lattice Gas Automata for the Navier-Stokes Equation. *Phys. Rev. Lett.* **56** (14), 1504, 1986.

[21] H. Chen, S. Chen, and W.H. Matthaeus. Recovery of the Navier-Stokes equations using a lattice-gas Boltzmann Method, *Phys. Rev. A*. **45**, 5339-5342, 1992.

[22] A.J.C. Ladd. Numerical simulation of particular suspensions via a discretized Boltzmann equation: Part 1 Theoretical foundation. *J. Fluid Mech.* 271, 258-309, 1994.

[23] S. Chen, G.D. Doolen. Lattice Boltzmann method for fluid flows. *Ann. Rev. Fluid. Mech.*, **30,** 329-364, 1998.

[24] D. Yu, R. Mei, L.S. Luo et al, Viscous flow computations with the method of lattice Boltzmann equation, Progress in Aerospace Sciences, 39 (2003) 329-367.

[25] T.C. Liu, Y.J. Ge, F.C. Cao. Turbulence Flow Simulation Based on the Lattice-Boltzmann Method Combined with LES. *Proceeding of the 12th International Conference on Wind Engineering*, Cairns, Australia, July, 2007.

[26] S. Chen, D. Martinez, and R. Mei. On boundary conditions in lattice Boltzmann methods, *Phys. Fluid*., **8**, 2527-2536, 1996.

[27] P.L. Bhatnagar, E.P. Gross, M. Kook. A Model for Collision Processes in Gases. I. Small Amplitude Processes in Charged and Neutral One-Component System, *Phys. Rev.*, 94,511-525,1954

[28] S. Chapman, T.G. Cowling. The Mathematical Theory of Non-Uniform Gases, Cambridge University Press, 1970.

[29] P.W. Bearman, E.D. Obasaju. An experimental study of pressure fluctuations on fixed and oscillating square-section cylinders. J. Fluid Mech., 119, 1982, 297-321.

[30] I. Taylor, V. Marco. Prediction of unsteady flow around square and rectangular section cylinders using a discrete vortex method. *J. Wind. Eng. Ind. Aero*, 82, 247-269, 1999.

[31] A. Santosh, S.C. Shyam. Entropic Lattice Boltzmann Simulation of the Flow Past Square Cylinder. *Int. J. Mod. Phys. C*, **15**(3), 435-445, 2004.

[32] J.H. Walther, A. Larsen. Two dimensional discrete vortex method for application to bluff body aerodynamics. *J. Wind. Eng. Ind. Aero*., 1997 (67), 183

[33] F.C. Cao, Numerical Simulation of Aeroelastic Problems in Bridge, Dissertation for ph. d., Shanghai, China, 1999, p. 92.

[34] M. Breuer. A challenging test case for large eddy simulation: high Reynolds number circular cylinder. *Proceedings of the first Turbulence and Shear Flow Phenomena*, Begelhouse Inc., New York, 735-741, 1999.

[35] R.D. Blevins. Flow Induced Vibration. Mechanism Industry Press. , Beijing, 1981.